ACTA MECHANICA SOLIDA SINICA 30 (2017) 241–247

Available online at www.sciencedirect.com

ScienceDirect

journal homepage: www.elsevier.com/locate/CAMSS

Molecular dynamics simulation of diffusion of nanoparticles in mucus

Jiuling Wang[a,b,c], *Xinghua Shi*[b,c,*]

[a] *LNM, Institute of Mechanics, Chinese Academy of Sciences, Beijing 100190, China*
[b] *CAS Key Laboratory for Nanosystem and Hierarchy Fabrication, CAS Center for Excellence in Nanoscience, National Center for Nanoscience and Technology, Chinese Academy of Sciences, Beijing 100190, China*
[c] *University of Chinese Academy of Sciences, Beijing 100049, China*

ARTICLE INFO

Article history:
Received 9 March 2017
Revised 31 March 2017
Accepted 31 March 2017
Available online 6 April 2017

Keywords:
Nanoparticle diffusion
Mucus penetration
Fibrous medium
Molecular dynamics simulation
Drug delivery

ABSTRACT

The rapid diffusion of nanoparticles (NPs) through mucus layer is critical for efficient transportation of NPs-loaded drug delivery system. To understand how the physical and surface properties of NPs affect their diffusion in mucus, we have developed a coarse-grained molecular dynamics model to study the diffusion of NPs in modeled mucus layer. Both steric obstruction and hydrodynamic interaction are included in the model capable of capturing the key characteristics of NPs' diffusion in mucus. The results show that both particle size and surface properties significantly affect the diffusivities of NPs in mucus. Furthermore, we find rodlike NPs can gain a higher diffusivity than spherical NPs with the same hydrodynamic diameter. In addition, the disturbed environment can enhance the diffusivity of NPs. Our findings can be utilized to design mucus penetrating NPs for targeted drug delivery system.

1. Introduction

Mucus is a continuously renewed, dynamic semipermeable viscoelastic gel produced by, and covering, mucous membranes. It protects our lung airways, gastrointestinal (GI) tracts, female reproductive tracts, eyes and other mucosal surfaces from entry of external fungi, bacteria and viruses [1]. Mucus is composed primarily of cross-linked and entangled mucin fibers secreted by goblet cells in the mucous membranes. The water content in mucus is within the range from 90% to 98%. Other components of the mucus include lipids, cell debris, macromolecules, enzymes, antibodies, DNA and electrolytes. All of these components together make mucus a highly heterogeneous fibrous medium. The thickness of the mucus layer varies from a few microns to several hundred microns, depending on the anatomical location [1,2]. The bulk viscosity of typical mucus is about 1000–10,000 times higher than that of water at low shear rates [3].

With the development of nanotechnology, nanoparticles (NPs)-based biomedical methods have become a promising way to diagnose and treat diseases [4]. A number of mucosal diseases could be treated more effectively and with fewer side effects if NPs could more uniformly and persistently deliver drug and gene to mucosal surfaces, such as sexually transmitted infections, cystic fibrosis, inflammatory bowel disease, and so on. Also, the oral administrated NPs-based drugs need to translocate through the intestinal mucus layer to enter into the circulatory system. However, conventional NPs are easily to be trapped in mucus by steric obstruction and rapidly removed from the body. Recently, Hanes et al. developed muco-inert NPs coated with a dense layer of low molecular poly(ethylene glycol) (PEG) and significantly increased transport rates of NPs in mucus [5-8]. Some recent studies have also shown that rodlike particles can gain

* Corresponding author.
E-mail address: shixh@nanoctr.cn (X. Shi).

http://dx.doi.org/10.1016/j.camss.2017.03.012
0894-9166/

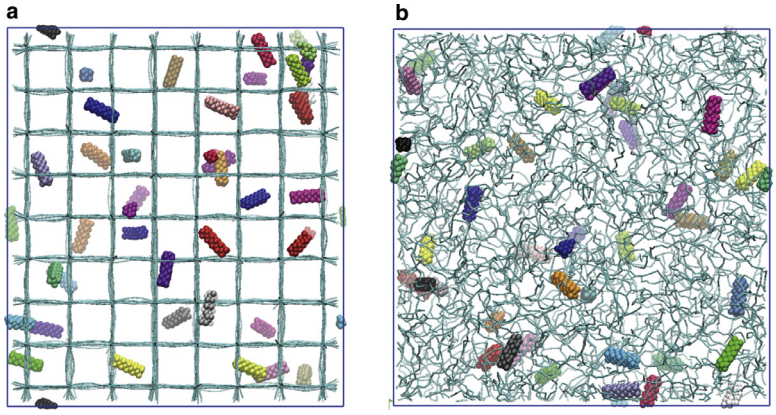

Fig. 1 – The simulation system. (a) and (b) are regular and random networks, respectively. Polymers are shown in cyan, 40 NPs are represented in a variety of colors, and water molecules are not shown for clarity.

superior transport capability in mucus compared with spheres of the same chemistry [9,10]. At present, it is imperative to understand how the physical and surface properties of NPs affect their transport through the mucus.

Theoretical analysis and computational simulations have been proven to be powerful in studying the transport of NPs in biological system. For example, molecular dynamics simulation and theoretical analysis have been used to study the translocation of NPs into the cells, and Monte Carlo simulations have been used to study the diffusion of NPs in the tumor interstitial matrix [11-14]. Due to the high heterogeneity of mucin network structure and multiple interactions between NPs and mucin fibers, it is almost impossible to elucidate the mechanism underlying the phenomenon of NPs' diffusion experimentally. In this case molecular dynamics simulation is highly suitable for studying how different factors affect the diffusion of NPs in the mucus. Here we have developed a coarse-grained molecular dynamics model to study the diffusion of NPs in mucus. Both steric obstruction and hydrodynamic interaction are included in the model, which is capable of capturing the key characteristics of NPs' diffusion in mucus [1,5,15-17]. Using this model, we have investigated the effects of particle size, shape, surface properties, and shear flow on the diffusion of NPs, and the results are consistent with the present experimental ones. Our model can be extended to study the effects of stiffness of NPs, pore size distribution of mucus, mucin fiber radius, and electrostatic interaction on the diffusion of NPs [18-21]. Our model provides a better understanding of the diffusion of NPs in mucus and could be used to design and optimize the NPs-based drug delivery system.

2. Simulation system and details

To simulate the diffusion of NPs in mucus, we constructed a system composed of cross-linked polymers, water and NPs. Both regular and random polymer network were used to represent the mucin fibers, as shown in Fig. 1. For regular network, the box size was $48\times54\times48\sigma^3$ (σ is the unit of length), and there were 208 polymer chains (9216 polymer beads) and 96,984 water beads in the system. The corresponding water content was about 91.3%. The distance between two adjacent fibers was 6σ. Different fibers were cross-linked by covalent bonds to simulate the entanglement and crosslinks of mucin fibers. For moderate random network, the box size was $50\times50\times50\sigma^3$, and there were 100 polymer chains (10,000 polymer beads) and 96,200 water beads in the system. The corresponding water content was about 90.6%. The polymer chains were cross-linked and randomly distributed in the system. In addition, we also constructed a sparse random network to compare with the moderate one, which consisted of 28 polymer chains (5600 polymer beads) and 100,600 water beads. In each simulation, 40 NPs were randomly placed in the system.

Within the polymer, the neighboring beads were connected by a harmonic spring with an equilibrium bond length of $r_0=\sigma$ and a spring constant of $k_b=50\varepsilon/\sigma^2$, where ε is the unit of energy. In order to show the obstructive action of mucin fibers on the movement of NPs, we constrained the mucus fibers during the simulations with a spring applied independently to each atom in polymer to tether it to its initial position. The spring constant was set at $k_{self}=20\varepsilon/\sigma^2$. By this method, polymer beads remained in the vicinity of their initial positions throughout the simulation. In this study, we constructed four types of NPs, i.e. spherical NPs with diameters of 2.1σ (NS2.1), 3.5σ (NS3.5), and 4.6σ (NS4.6), and rodlike NPs with size of $2.1\times4.6\sigma$ (NR2.1*4.6). These NPs were created by a face-centered cubic (fcc) lattice with a Lennard–Jones reduced density of 8. The NS3.5 and NR2.1*4.6 had the same hydrodynamic diameter, which meant that they had the same diffusion coefficients in water. The single NP was constrained as a rigid body during the simulation. In all simulations, the Lennard–Jones (LJ) potential and Weeks–Chandler–Anderson (WCA) potential were used as follows to describe the nonbonded interactions $V(r)$ between two beads,

$$V(r)=4\alpha\varepsilon\left\{\left[\left(\frac{\sigma}{r}\right)^{12}-\left(\frac{\sigma}{r}\right)^{6}\right]-\left[\left(\frac{\sigma}{r_c}\right)^{12}-\left(\frac{\sigma}{r_c}\right)^{6}\right]\right\},\ r<r_c, \quad (1)$$

where r is the distance between two beads, α is the tunable interaction strength, and r_c is the cutoff distance set as 2.5σ for LJ potential and $2^{1/6}\sigma$ for WCA potential. The interaction parameters between different beads are listed in Table 1.

During the simulation, periodic boundary condition was applied in all three directions. The velocity-Verlet algorithm

Table 1. – Interaction parameters for different particle types.

Bead type	Bead type	Interaction	α
Polymer	Polymer	WCA	1.0
	Water	LJ	2.0
	NPs	WCA	0.5
Water	Water	LJ	2.0
	NPs	LJ	1.5
NPs	NPs	WCA	0.5

was utilized to perform the time integration. The integration time step was $\delta t=0.01\tau$, where $\tau = \sqrt{m\sigma^2/\varepsilon}$ was the unit of time. In order to obtain the effective time of τ, we compared the diffusivity of NS3.5 calculated by our simulation with that predicted by theoretical equation $D = \frac{k_B T}{6\pi \cdot a \cdot \eta}$, where a is the radius of the spherical particle (σ, the unit of length, was set at 1 nm, and a was 3.5 nm) and η is the viscosity of the suspending medium (for water, $\eta = 1.0 \times 10^{-3}$Pa · s). Then the effective time of τ was about 60 ps. We used the Nose–Hoover barostat to control the system pressure at $P=0$, and the Nose–Hoover thermostat to control the system temperature at $k_B T=1.1\varepsilon$, where k_B is the Boltzmann constant, and T is temperature. All the simulations were performed using the LAMMPS code [22].

The time-averaged mean square displacement (MSD) was calculated using the following equation,

$$\mathrm{MSD}_t = \left\langle (x_{t_0+t} - x_{t_0})^2 + (y_{t_0+t} - y_{t_0})^2 + (z_{t_0+t} - z_{t_0})^2 \right\rangle_{t_0} \quad (2)$$

where x, y and z represent the centroid coordinates of the NPs, t_0 is the selected initial time, and t is time lag. For each simulation, the total simulation time was $80{,}000\tau$. We repeated the simulation 8 times with different starting configurations and obtained the mean MSD of NPs.

3. Results and discussion

3.1. *Size and shape effect*

In real mucus the pore size is about a few hundred nanometers [7], and larger NPs can be strongly hindered by the dense fibers of mucus. Here we investigated the effect of size and shape of NPs on their diffusion in mucus [15,17]. The mean square displacements (MSDs) of four types of NPs in random network are presented in Fig. 2a. Obviously, with the increase of particle size, the MSDs of particles gradually decrease, which is consistent with our intuition. For NS2.1, the MSD increases linearly, whereas the increase of MSD for NS3.5 slows down with elapsed time. This means that the diffusion mode changes from normal diffusion to sub-diffusion as the particle size increases [23]. For NS4.6, the MSD is three orders of magnitude smaller than that of NS2.1, indicating that particles above a certain size would be completely trapped in the network structure. Recent experimental observations have shown that, although 500-nm particles can penetrate rapidly through the human cervicovaginal mucus, 1-μm particles will be trapped in the mucus due to the steric obstruction, which is consistent with our results [7]. The rodlike particles NR2.1*4.6 which have the same hydrodynamic size as spherical particles NS3.5 experience a nearly normal diffusion in mucus. Accordingly, they achieve a higher diffusivity in mucus, and the enhanced diffusivity is attributed to the rotational dynamics of rodlike NPs facilitated by the mucin fibers [10].

Consider that the NPs may experience anomalous diffusion in a short time, we obtained the diffusivity of NPs by linear fitting the MSD versus time lag from $20{,}000\tau$ to $60{,}000\tau$, as shown in Fig. 3a. The slope of fitting line is denoted by k, then the diffusivity $D=k/6$. The calculated diffusivities are shown in Table. 2. Since these NPs have different hydrodynamic sizes, we also compared the normalized diffusivities of these NPs. The diffusivity of NPs in water is denoted by D_w, and the normalized diffusivity κ is defined as $\kappa = D/D_w$. The κ for different NPs in random network are shown in Fig. 3b. In both moderate and sparse networks, κ decreases with increasing particle size, indicating that the network structure has a stronger hindered effect on the movement of particles. For moderate network, the steric obstruction is more significant. For example, the normalized diffusivity of NS3.5 is 39% of that of NS2.1 in sparse network, whereas the ratio is reduced to 9.8% in moderate network. We also note that the normalized diffusivity of NR2.1*4.6 is 3.8-fold higher than that of NS3.5 in moderate network, and 1.4-fold higher in sparse network. Therefore, rodlike NPs can gain a higher diffusivity than spherical NPs in a certain range of polymer concentration [10].

3.2. *NPs-mucin fibers interaction*

Steric obstruction and adhesion are the main factors that prevent the penetration of NPs through the mucus [1].

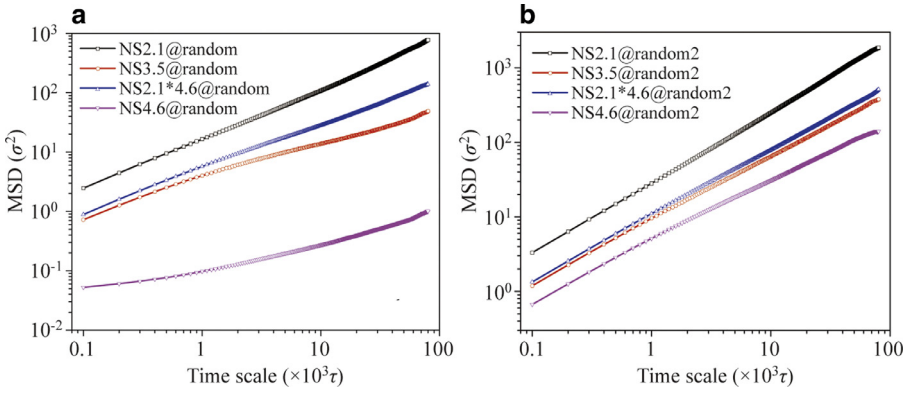

Fig. 2 – Log-log plot of the MSDs of NPs in (a) moderate and (b) sparse random networks.

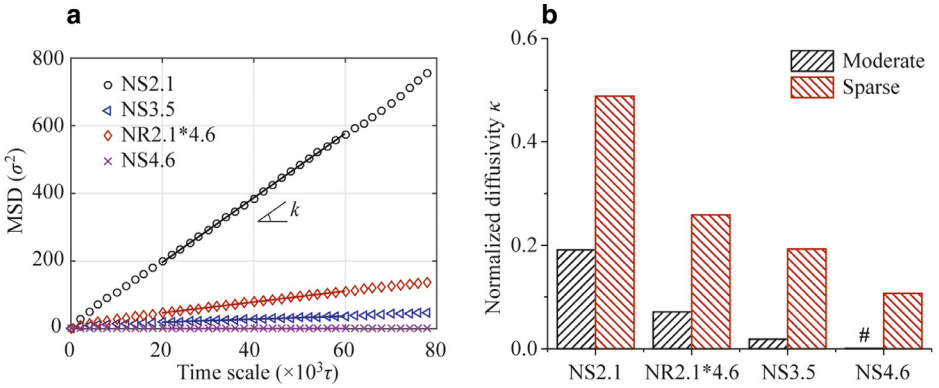

Fig. 3 – (a) Normal plot of the MSDs of NPs in moderate random network. Solid lines are linear fitting the MSD versus time lag from 20,000τ to 60,000τ, k is the slope of fitting line, then $D=k/6$. (b) Normalized diffusivity of NPs in moderate and sparse random networks. The symbol # indicates that the normalized diffusivity of NS4.6 is close to zero.

Table 2. – The diffusivity of NPs in random network.

Diffusivity ($10^{-3}\sigma^2/\tau$)	NS2.1	NS3.5	NR2.1*4.6	NS4.6
Moderate network	1.587	0.073	0.268	0.002
Sparse network	4.047	0.751	0.974	0.296
Water	8.290	3.897	3.760	2.760

Table 3. – The diffusivity of NPs in regular network with different polymer-NPs interactions.

Diffusivity ($10^{-3}\sigma^2/\tau$)	WCA	LJ, $\alpha=0.5$	LJ, $\alpha=1.0$	LJ, $\alpha=1.5$
NS3.5	0.075	0.108	0.121	0.031
NR2.1*4.6	0.370	0.367	0.419	0.044

Recent studies have shown that NPs coated with low molecular poly(ethylene glycol) (PEG) can significantly increase transport rates of NPs in mucus [5-7]. These mucus-penetrating particles (MPP) mimic the essential surface properties of viruses, which are densely coated with both positively and negatively charged groups, to avoid mucin adhesion. In the previous section, we have used the weakly repulsive WCA potential to describe the interaction between polymers and NPs, so as to study the diffusion of MPP in mucus. Here we also studied the effect of NPs-polymer interaction on the diffusion of NPs. We changed the interaction from WCA to LJ potential and tuned the interaction strength α from 0.5 to 2.0, the corresponding MSDs of NPs are shown in Fig. 4, and the diffusivities are listed in Table 3.

For spherical particles NS3.5, the diffusivity increases slightly with the increase of interaction strength. However, the diffusivity decreases sharply when the interaction strength α reaches 1.5. For rodlike particles NR2.1*4.6, the diffusivity does not change significantly when α is below 1.0, while drops remarkably when α reaches 1.5. The rapid decreases in diffusivity of both NPs are due to the attraction between the particles and the polymer, which causes the particles to adsorb onto the polymer and prohibits their diffusion. The snapshots in the simulation clearly show the adsorption of particles on the polymer (Fig. 5). At this interaction strength, a small fraction of NPs can detach from the polymer, diffuse through the water, and re-adsorb onto the polymer during the simulation [24,25]. When the interaction strength α increases to 2.0, all the

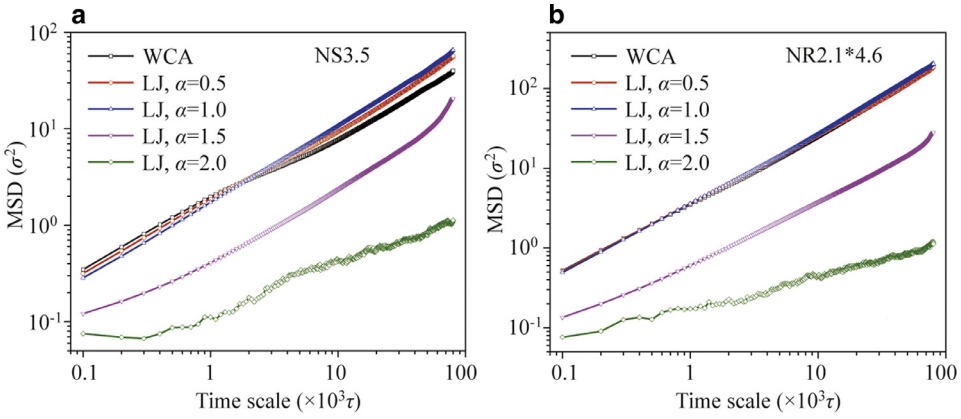

Fig. 4 – The MSDs of NPs in regular network with different polymer-NPs interactions. (a) and (b) are for NS3.5 and NR2.1*4.6, respectively.

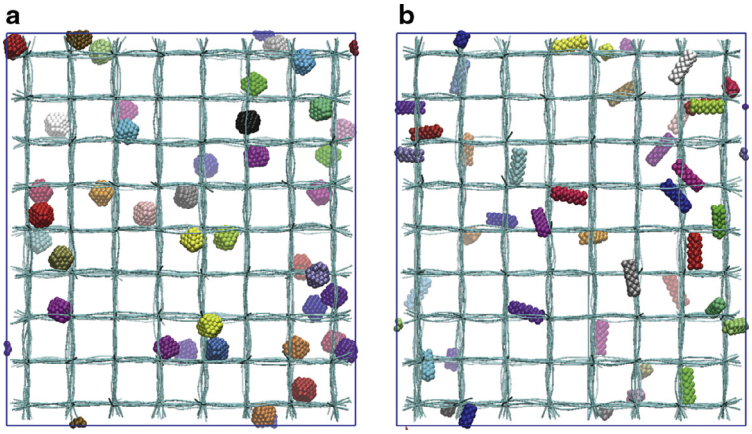

Fig. 5 – Snapshots of NPs in regular network when the polymer-NPs interaction strength α is 1.5. (a) and (b) are for NS3.5 and NR2.1*4.6, respectively. All NPs are in the vicinity of the polymers, which is significantly different from the random distribution of NPs in the system at the initial moment.

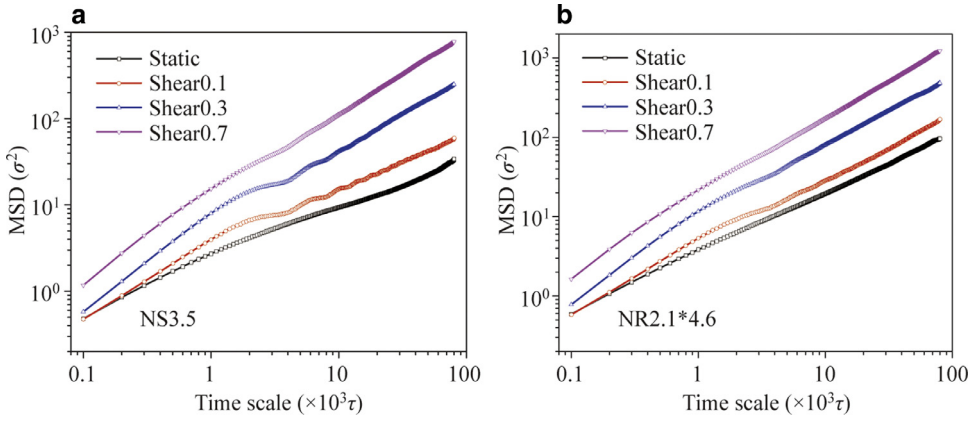

Fig. 6 – The MSDs of NPs under shear flow in random network. (a) and (b) are for NS3.5 and NR2.1*4.6, respectively. shear0.1, shear0.3 and shear0.7 denote that the coefficient F_{max} in drag force formula is 0.1, 0.3 and 0.7.

particles are firmly adsorbed onto the polymer surface, and only vibrate under disturbance.

3.3. *Diffusion under shear flow*

In the human GI tract, mucus is continuously secreted at a rate of 1–100 μm/s. And in respiratory tract, mucociliary transport velocity is about 10–100 μm/s [2]. In order to simulate the effects of GI peristalsis and mucus secretion on the diffusion of NPs, we have also studied the diffusion of NPs in random polymer network under oscillatory shear flow.

We applied shear flow in the x-direction by adding a drag force $F_{add} = F_{max} \cdot y\varepsilon/(L_y\sigma)$ to each water bead in the simulation system, where y and L_y are the coordinates of water beads and the box size along the y-direction, respectively, F_{max} is a coefficient and ε is the unit of energy. We reversed the force direction every 200,000 time steps, through which the oscillatory shear flow along the x-direction was applied. We have changed the magnitude of shear force to observe the movement of NPs. The MSDs and effective lateral diffusivities of NPs under shear flow are shown in Fig. 6 and Table 4, respectively. During the calculation of MSD, we have excluded the movement of NPs along the x-direction to focus on the movement of NPs in the yz-plane. The effective lateral diffusivity is calculated by the formula $D_e = k/4$, where k is the slope of the fitting line of MSD versus time lag. It contains not only the movement of NPs by diffusion, but also the motion of NPs under the influence of the shear flow. With the increase of shear force, the movement ability of NPs in the yz-plane is enhanced significantly (Table 4). We attribute this to the shear-flow-enhanced frequency of which NPs contact with polymers and change the movement direction. Such collisions could effectively increase the effective diffusivity of NPs. In order to

Table 4. – The effective lateral diffusivity of NPs under shear flow in random network and water.

Diffusivity ($10^{-3}\sigma^2/\tau$)	Static	$F_{max}=0.1$	$F_{max}=0.3$	$F_{max}=0.7$
NS3.5@network	0.075	0.145	0.720	2.405
NR2.1*4.6@network	0.370	0.500	1.387	3.702
NS3.5@water	3.897	4.062	2.059	
NR2.1*4.6@water	3.760	4.516	3.295	

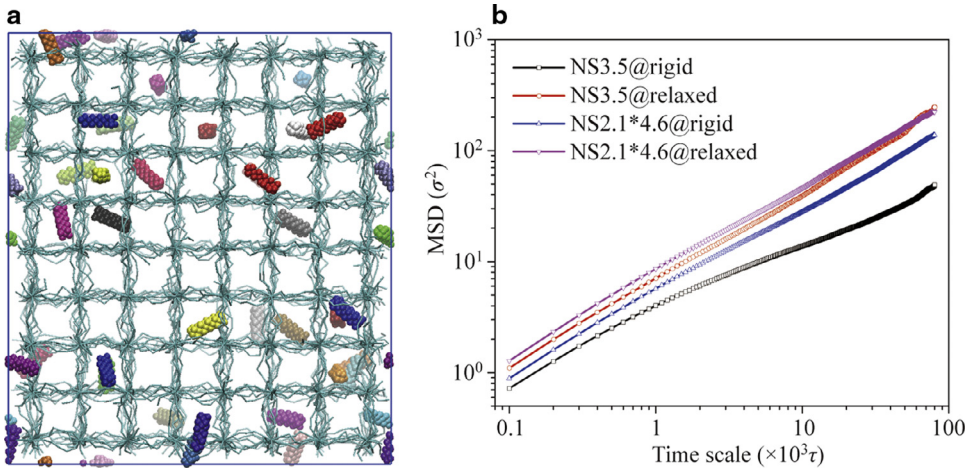

Fig. 7 – (a) A snapshot of NR2.1*4.6 in regular network when the polymer beads were relaxed. (b) The MSD of NPs in rigid and relaxed regular network.

confirm the role of polymer network in shear-flow-enhanced motility, we also studied the effect of shear flow on lateral movement of NPs in water with the results shown in Table 4. When the velocity of shear flow is low ($F_{max}=0.1$), the effective diffusivities of NS3.5 and NR2.1*4.6 increase by 4% and 20%, respectively. However, as the flow velocity becomes higher ($F_{max}=0.3$), the effective diffusivities of two NPs decrease by 47% and 12%, respectively. These results indicate that the flow would cause rodlike NPs to move faster in the lateral direction than the spherical ones. Also the effective diffusivities of both NPs are flow-rate-dependent. Recent studies have shown that spherical particles have smaller lateral displacement than ellipsoidal particles in a flowing straight tube [26,27]. Therefore, we draw a conclusion that the perturbed external environment would dramatically increase the lateral motility of NPs in the fibrous medium, but not in water [21].

3.4. *Rigidity of mucin fibers*

In previous simulations, we have constrained all the polymer beads to simulate rigid mucin fibers. Recent experimental studies have demonstrated that the rigidity of mucin scaffold could affect the penetration of particles through mucus [20]. Here, we relaxed the mucin fibers by constraining only the cross-linked beads, and setting the bond length of the adjacent beads (at a separation of 1σ) to $1.2\,\sigma$. It is seen that the diffusivities of NPs remarkably increase after the relaxation of polymer (Fig. 7), which is in good agreement with the results of the recent experimental investigation [20]. In addition, the difference in the diffusivity between the spherical particles (NS3.5) and the rodlike particles (NR2.1*4.6) becomes smaller due to the effectively enlarged pore size.

4. Conclusions

In summary, we have established a coarse-grained molecular dynamics simulation model to simulate the diffusion of NPs in mucus. The model has shown the power to reproduce mobility of NPs in mucus in the following respects. Firstly, our model has reproduced the effect of particle size on particle diffusion in mucus: as the particle size increases, the normalized diffusivity decreases, and NPs beyond a certain size are completely trapped in the network. Secondly, our model can study the effect of adhesion between NPs and mucin fibers on their diffusion: as the adhesion increases to a certain value, the diffusivity decreases dramatically. Thirdly, we have investigated the effect of shear flow on the diffusion of NPs in the fibrous medium, with the results shown that external perturbations can contribute to particle diffusion. Fourthly, our model have reproduced the phenomenon that rigid mucin scaffold limits the diffusion of NPs in mucus, which agrees well with the experimental results [20]. In addition, our model can be easily extended to study the effects of heterogeneous pore structures, mucin fiber radius, and electrostatic interaction on the diffusion of NPs in mucus. The model can help us in designing NPs penetrating through the mucus for drug delivery.

Acknowledgments

We are grateful for the financial support from the National Natural Science Foundation of China (No. 11422215, 11272327 and 11672079). The computation is mainly supported by the Supercomputing Center of Chinese Academy of Sciences (SCCAS).

REFERENCES

[1] S.K. Lai, Y.Y. Wang, J. Hanes, Mucus-penetrating nanoparticles for drug and gene delivery to mucosal tissues, Adv. Drug Delivery Rev. 61 (2009) 158–171.
[2] R.A. Cone, Barrier properties of mucus, Adv. Drug Delivery Rev. 61 (2009) 75–85.
[3] S.K. Lai, Y.Y. Wang, D. Wirtz, J. Hanes, Micro- and macrorheology of mucus, Adv. Drug Delivery Rev. 61 (2009) 86–100.
[4] T.L. Doane, C. Burda, The unique role of nanoparticles in nanomedicine: imaging, drug delivery and therapy, Chem. Soc. Rev. 41 (2012) 2885–2911.

[5] S.K. Lai, D.E. O'Hanlon, S. Harrold, S.T. Man, Y.Y. Wang, R. Cone, J. Hanes, Rapid transport of large polymeric nanoparticles in fresh undiluted human mucus, Proc. Natl. Acad. Sci. USA 104 (2007) 1482–1487.
[6] Y.Y. Wang, S.K. Lai, J.S. Suk, A. Pace, R. Cone, J. Hanes, Addressing the PEG mucoadhesivity paradox to engineer nanoparticles that "slip" through the human mucus barrier, Angew. Chem.-Int. Ed. 47 (2008) 9726–9729.
[7] S.K. Lai, Y.Y. Wang, K. Hida, R. Cone, J. Hanes, Nanoparticles reveal that human cervicovaginal mucus is riddled with pores larger than viruses, Proc. Natl. Acad. Sci. USA 107 (2010) 598–603.
[8] B.C. Tang, M. Dawson, S.K. Lai, Y.Y. Wang, J.S. Suk, M. Yang, P. Zeitlin, M.P. Boyle, J. Fu, J. Hanes, Biodegradable polymer nanoparticles that rapidly penetrate the human mucus barrier, Proc. Natl. Acad. Sci. USA 106 (2009) 19268–19273.
[9] V.P. Chauhan, Z. Popovic, O. Chen, J. Cui, D. Fukumura, M.G. Bawendi, R.K. Jain, Fluorescent nanorods and nanospheres for real-time in vivo probing of nanoparticle shape-dependent tumor penetration, Angew. Chem.-Int. Ed. 50 (2011) 11417–11420.
[10] M. Yu, J. Wang, Y. Yang, C. Zhu, Q. Su, S. Guo, J. Sun, Y. Gan, X. Shi, H. Gao, Rotation-facilitated rapid transport of nanorods in mucosal tissues, Nano Lett. 16 (2016) 7176–7182.
[11] K. Yang, Y.Q. Ma, Computer simulation of the translocation of nanoparticles with different shapes across a lipid bilayer, Nat. Nanotechnol. 5 (2010) 579–583.
[12] J.L. Wang, H.M. Yao, X.H. Shi, Cooperative entry of nanoparticles into the cell, J. Mech. Phys. Solids 73 (2014) 151–165.
[13] J.L. Wang, Y.J. Wei, X.H. Shi, H.J. Gao, Cellular entry of graphene nanosheets: the role of thickness, oxidation and surface adsorption, RSC Adv. 3 (2013) 15776–15782.
[14] T. Stylianopoulos, B. Diop-Frimpong, L.L. Munn, R.K. Jain, Diffusion anisotropy in collagen gels and tumors: the effect of fiber network orientation, Biophys. J. 99 (2010) 3119–3128.
[15] S.S. Olmsted, J.L. Padgett, A.I. Yudin, K.J. Whaley, T.R. Moench, R.A. Cone, Diffusion of macromolecules and virus-like particles in human cervical mucus, Biophys. J. 81 (2001) 1930–1937.
[16] T. Ando, J. Skolnick, Crowding and hydrodynamic interactions likely dominate in vivo macromolecular motion, Proc. Natl. Acad. Sci. USA 107 (2010) 18457–18462.
[17] O. Lieleg, K. Ribbeck, Biological hydrogels as selective diffusion barriers, Trends Cell Biol. 21 (2011) 543–551.
[18] A. Pluen, P.A. Netti, R.K. Jain, D.A. Berk, Diffusion of macromolecules in agarose gels: comparison of linear and globular configurations, Biophys. J. 77 (1999) 542–552.
[19] T. Stylianopoulos, M.Z. Poh, N. Insin, M.G. Bawendi, D. Fukumura, L.L. Munn, R.K. Jain, Diffusion of particles in the extracellular matrix: the effect of repulsive electrostatic interactions, Biophys. J. 99 (2010) 1342–1349.
[20] J. Kirch, A. Schneider, B. Abou, A. Hopf, U.F. Schaefer, M. Schneider, C. Schall, C. Wagner, C.M. Lehr, Optical tweezers reveal relationship between microstructure and nanoparticle penetration of pulmonary mucus, Proc. Natl. Acad. Sci. USA 109 (2012) 18355–18360.
[21] R. Agarwal, P. Jurney, M. Raythatha, V. Singh, S.V. Sreenivasan, L. Shi, K. Roy, Effect of shape, size, and aspect ratio on nanoparticle penetration and distribution inside solid tissues using 3D spheroid models, Adv. Healthcare Mater. 4 (2015) 2269–2280.
[22] S. Plimpton, Fast parallel algorithms for short-range molecular dynamics, J. Comput. Phys. 117 (1995) 1–19.
[23] F. Hofling, T. Franosch, Anomalous transport in the crowded world of biological cells, Rep. Progress Phys. 76 (2013) 046602.
[24] R. Walder, N. Nelson, D.K. Schwartz, Single molecule observations of desorption-mediated diffusion at the solid-liquid interface, Phys. Rev. Lett. 107 (2011) 156102.
[25] M.J. Skaug, J. Mabry, D.K. Schwartz, Intermittent molecular hopping at the solid-liquid interface, Phys. Rev. Lett. 110 (2013) 256101.
[26] E. Gavze, M. Shapiro, Motion of inertial spheroidal particles in a shear flow near a solid wall with special application to aerosol transport in microgravity, J. Fluid Mech. 371 (1998) 59–79.
[27] P. Decuzzi, R. Pasqualini, W. Arap, M. Ferrari, Intravascular delivery of particulate systems: does geometry really matter? Pharm. Res. 26 (2009) 235–243.